Inorganic Chemistry

Article

pubs.acs.org/IC

Evidence for Bidirectional Noninnocent Behavior of a Formazanate Ligand in Ruthenium Complexes

Abhishek Mandal,[†] Brigitte Schwederski,[‡] Jan Fiedler,[§] Wolfgang Kaim,*[,‡] and Goutam Kumar Lahiri*[,†]

[†]Department of Chemistry, Indian Institute of Technology Bombay, Powai, Mumbai-400076, India

[‡]Institut für Anorganische Chemie, Universität Stuttgart, Pfaffenwaldring 55, D-70550 Stuttgart, Germany

[§]J. Heyrovský Institute of Physical Chemistry, v.v.i., Academy of Sciences of the Czech Republic, Dolejškova 3, CZ-18223 Prague, Czech Republic

Supporting Information

ABSTRACT: Redox series of the complexes $[Ru(L)(L')_2]^n$, L = 1,5-diphenyl-3-(4-tolyl)-formazanate and L′ = 2,4-pentanedionate ($acac^-$), 2,2′-bipyridine (bpy), or 2-phenylazopyridine (pap), were studied by cyclic and differential pulse voltammetry and by TD-DFT-supported spectroelectrochemistry (UV−vis−NIR, EPR). The precursors $[Ru^{III}(L^-)(acac^-)_2]$, $[Ru^{II}(L^-)(bpy)_2]ClO_4$, and $[Ru^{II}(L^-)(pap)_2]ClO_4$ were identified in their indicated oxidation states by X-ray crystal structure determination. The six-membered formazanato-ruthenium chelate rings have an envelope conformation with puckering of the metal. DFT calculations indicate a pronounced sensitivity of the N−N bond lengths toward the ligand oxidation state. Several electrochemically accessible charge states were analyzed, and the derived oxidation numbers Ru^{II}, Ru^{III}, or Ru^{IV}, L′ or $(L')^{\bullet-}$, and L^-, $L^{\bullet 2-}$, or the new formazanyl ligand $L^\bullet$ for the two-way noninnocent formazanate reflect the increasing acceptor effect of the ancillary ligands L′ in the series $acac^-$ < bpy < pap.

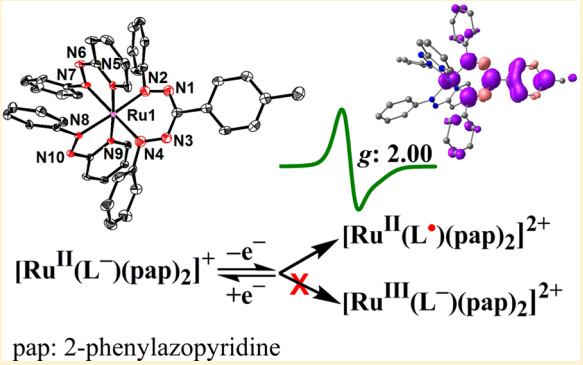

INTRODUCTION

Nitrogen-rich redox-active molecules have been prominent among the series of noninnocently behaving ligands.[1] Representative examples are the 1,2,4,5-tetrazines,[2] azo compounds,[3] verdazyls,[4] and triazenides.[5] Recently, formazanates were shown to occur as anions or dianions in zinc(II) complexes.[6] Coordination compounds of formazanate ligands have long been studied in connection with industrial dyes and other colorimetric applications;[7] among the metals and nonmetals employed were Cu, B, Co, Pd, and Ni.[7,8]

Complexes of formazanate ligands with ruthenium were not much investigated,[9] although the interaction of ruthenium (in the +I to +IV oxidation states)[10] with noninnocently behaving ligands can offer a rich and challenging chemistry, as demonstrated for compounds of nitrosyl,[11] α-diimine,[12] or quinone-type ligands.[13]

We therefore reacted the 1,5-diphenyl-(4-tolyl)-formazane (LH) with appropriate ruthenium reagents to produce the structurally characterized complexes $[Ru^{III}(L^-)(acac^-)_2]$, $[Ru^{II}(L^-)(bpy)_2]ClO_4$, and $[Ru^{II}(L^-)(pap)_2]ClO_4$ (Figure 1). Their electron transfer response with particular attention given to the possible noninnocence of L was studied using EPR and UV−vis−NIR spectroelectrochemistry,[14] allowing us to probe the potential of such systems for noninnocent ligand-based reactions.[15]

The formazanate ions belong to the same class of chelate ligands as the β-diketonates **I** (cf., "$acac^-$" or the related β-diketiminato ligands **II** ($NacNac^-$).[8c,16] The latter were shown to have a potential for noninnocent behavior, as evident from the "hidden noninnocence" of an oxidized nickel complex.[16] The replacement of O donors by NR in **I** → **II** causes increased basicity and steric shielding, which is also true for formazanates **III**. Furthermore, these ligands **III** have two CR functions replaced by N, whereas the remaining carbon atom in the chelate ligand is frequently carrying substituents.[8]

The systems **I**−**III** form six-membered chelate rings, which is relatively uncommon for noninnocent ligands.[16−18]

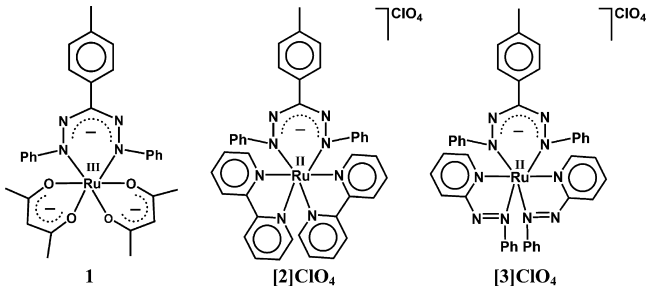

Figure 1. Representation of complexes.

Received: June 23, 2015
Published: August 5, 2015

© 2015 American Chemical Society

DOI: 10.1021/acs.inorgchem.5b01408
Inorg. Chem. 2015, 54, 8126−8135

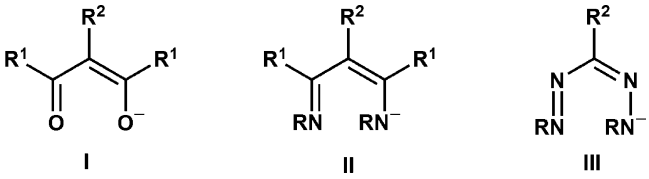

RESULTS AND DISCUSSION

Synthesis and Characterization. The compounds **1**, [**2**]ClO_4, and [**3**]ClO_4 (Figure 1) were obtained by reacting 1,5-diphenyl-3-*p*-tolylformazan (HL) with the ethanolic solution of the metal precursors *cis*-$Ru(acac)_2(CH_3CN)_2$, *cis*-$[Ru(bpy)_2(EtOH)_2](ClO_4)_2$, and *ctc*-$[Ru(pap)_2(EtOH)_2](ClO_4)_2$ (*ctc*: *cis*−*trans*−*cis* with respect to EtOH, pyridine, and azo nitrogens, respectively), in the presence of NEt_3 as a base and purified via column chromatography using silica gel. The presence of three negatively charged ligands (two $acac^-$ and formazanate) has facilitated the selective stabilization of Ru(III) in **1** under aerobic reaction conditions as has been observed earlier in $\{Ru(acac)_2\}$ containing complexes.[19] Analytical and mass spectrometric data confirm the molecular composition (Experimental Section and Figure S1).

Molecular Structures. The isolated compounds were **1**, [**2**]ClO_4, and [**3**]ClO_4, which could be characterized by single-crystal X-ray crystallography (Figures 2−4, Tables 1−3, Figure S2 and Tables S1−S5). As confirmed by the EPR signal (Figure 5) and by the ^1H NMR behavior showing partly broadened features (Figure S3a and Experimental Section), the neutral **1** is paramagnetic with the unpaired electron delocalized over the metal (formally Ru^{III}) and the triaryl-formazanate ligand (see EPR discussion and Figure 6). The ^{13}C NMR spectra of the complexes are shown in Figure S4a−c. The structure data are confirmed largely by the results from DFT calculations (Tables 1−3, Tables S3−S5 and Figure S5). A set of reference calculations for the noncoordinated redox series $L^•$, L^-, $L^{•2-}$ (Table 4) suggests particular sensitivity of the N−N bond lengths, similarly to 1,2,4,5-tetrazines[2] (for the experimental molecular structure of HL, see ref 8c).

The diamagnetic compounds [**2**]ClO_4 and [**3**]ClO_4 are EPR silent and exhibit corresponding $^1H/^{13}C$ NMR spectra (Figures S3b,c and S4b,c and Experimental Section). Compound [**2**]ClO_4 crystallizes with two independent cationic molecules

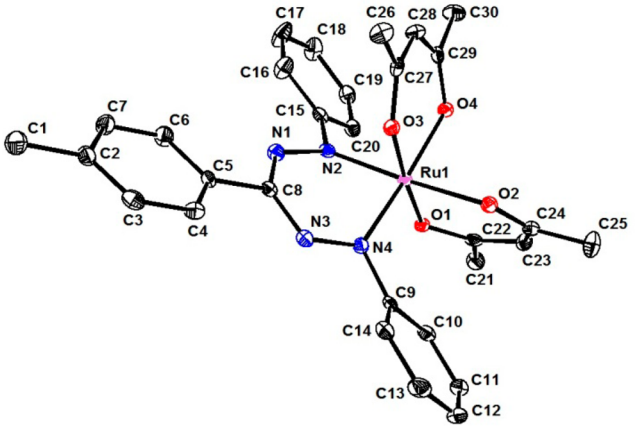

Figure 2. Molecular structure of **1** in the crystal. Ellipsoids are drawn at the 50% probability level. Hydrogen atoms are removed for clarity.

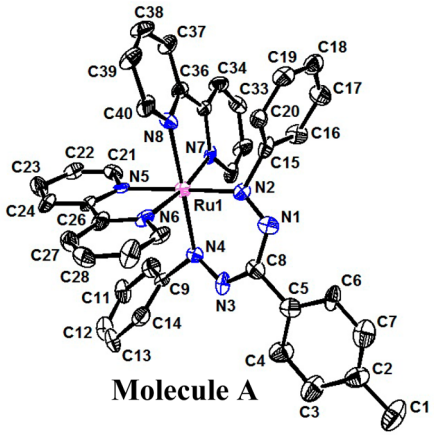

Figure 3. Cationic part of [**2**]ClO_4 (molecule A) in the crystal. Ellipsoids are drawn at the 50% probability level. Hydrogen atoms are removed for clarity.

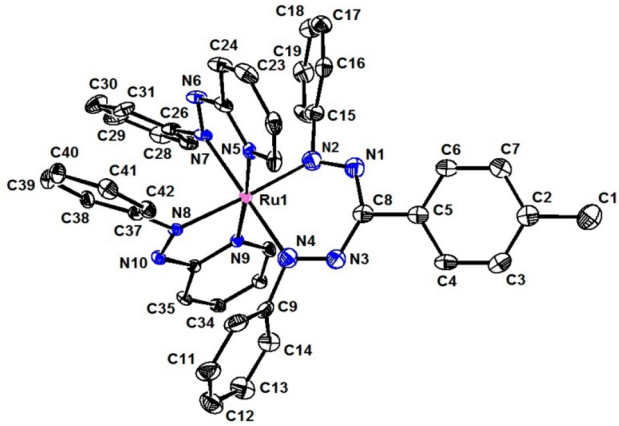

Figure 4. Cationic part of [**3**]ClO_4 in the crystal. Ellipsoids are drawn at the 20% probability level. Hydrogen atoms are removed for clarity.

A and **B** in the asymmetric unit (Figure 3 and Figure S2), both having very similar bond parameters.

The comparison of Ru−N(L), NN, and NC intrachelate bond lengths within the series of complexes reveals a distinct trend on replacing the more donating $acac^-$ coligands by weakly (bpy) or strongly (pap) π-accepting ancillary ligands. The average Ru−N bond lengths to the formazanate increase by about 0.1 Å (1.96 → 2.07 Å) in the order **1** < $\mathbf{2}^+$ < $\mathbf{3}^+$, indicating diminished electrostatic attraction as illustrated by the oxidation state assignments (Scheme 1). While the average NN distances decrease along that series by about 0.07 Å (1.32 → 1.25 Å), the intrachelate NC bonds grow longer by the same amount (1.35 → 1.42 Å), in agreement with lowered negative charge, that is, diminishing contributions from the $L^{•2-}$ form and more contributions from a $L^•$ formulation. Previous experimental data[6,8] have yielded typical NN bond lengths of 1.31 Å and intrachelate CN distances of 1.34 Å for monoanionic formazanate ligands, shifting to 1.36 Å for the NN bond on reduction to the dianionic state, whereas the CN bonds remain unchanged.[6] Our DFT calculations on various charged forms of the free ligands confirm this metric correlation (Table 4), yielding NN bond lengthening/shortening from about 1.30 to 1.34/1.28 Å on reduction/oxidation, while the intraligand CN distances exhibit less variation. According to this, there is a notable charge shift from L^- to the strongly π-

DOI: 10.1021/acs.inorgchem.5b01408
Inorg. Chem. 2015, 54, 8126−8135

Table 1. Selected Experimental and DFT Calculated Bond Lengths (Å) for 1^n

	X-ray	DFT		
bond lengths	**1**	$\mathbf{1}^+$ (S = 0)	**1** (S = 1/2)	$\mathbf{1}^-$ (S = 0)
Ru1−N2	1.9606(19)	1.991	2.014	2.044
Ru1−N4	1.9720(19)	2.026	2.014	2.049
Ru1−O1	2.0357(14)	2.082	2.090	2.104
Ru1−O2	2.0648(16)	2.059	2.107	2.129
Ru1−O3	2.0169(14)	2.044	2.053	2.092
Ru1−O4	2.0538(15)	2.050	2.086	2.130
N1−N2	1.320(2)	1.309	1.298	1.295
N3−N4	1.312(3)	1.280	1.291	1.296
C8−N1	1.342(3)	1.340	1.345	1.350
C8−N3	1.354(3)	1.377	1.354	1.350
C9−N4	1.443(3)	1.430	1.437	1.429
C15−N2	1.441(3)	1.420	1.436	1.430
C1−C2	1.509(3)	1.506	1.510	1.512
C2−C3	1.392(3)	1.405	1.401	1.401
C2−C7	1.395(3)	1.408	1.402	1.402
C3−C4	1.385(3)	1.388	1.392	1.393
C4−C5	1.395(3)	1.411	1.406	1.408
C5−C6	1.396(4)	1.412	1.406	1.409
C5−C8	1.487(3)	1.458	1.484	1.487
C6−C7	1.387(4)	1.386	1.391	1.392

accepting pap ligands in system $\mathbf{3}^n$ with a $L^{\bullet}/(pap^{\bullet-})$ ligand set as a limiting formulation.

The six-membered chelate rings show a distinct puckering with the metal being situated about 0.75 Å (**1**), 0.30 Å ($\mathbf{2}^+$), or 0.45 Å ($\mathbf{3}^+$) above the respective best planes (Table S6). While the *N*-phenyl groups in positions 1 and 5 are significantly twisted by about 60° (average, Table S7), the unhindered *p*-tolyl group in 3-position is more coplanar with the N_2CN_2 formazanate moiety (average twist angle 16°).

Despite the presence of a redox-active metal and of the potentially noninnocent coligands bpy and pap, we set out to probe the potential for noninnocent behavior of the formazanate ligand in complexes **1**, [**2**]ClO_4, and [**3**]ClO_4. The multistep electron transfer behavior of the compounds is illustrated by cyclic and differential pulse voltammetry (Figure 7, Table 5).

To assign the sites of individual redox processes, we used EPR (Figures 5 and 8, Table 6) and UV−vis−NIR spectroelectrochemistry (Figures 9−11, Tables S8−S10) as experimental information in conjunction with calculation results of spin densities (DFT, Figure 6, Table 7), electronic transitions (TD-DFT, Tables S8−S10), and MO compositions in accessible redox states (Tables S11−S24).

Compound **1** exhibits one reversible oxidation and one reversible reduction. Compounds [**2**]ClO_4 and [**3**]ClO_4 show also one reversible oxidation but display several reduction waves, due to the presence of reducible bpy or pap coligands. In accordance with the stronger acceptor pap and in agreement with the EPR and UV−vis−NIR data (cf., below), the facilitated reduction of [**3**]ClO_4 is attributed to the pap ligands as sites of the first electron additions. Conversely, the oxidation potential is shifted anodically for [**3**]ClO_4 as compared to [**2**]ClO_4. Irreversible second oxidations are observed for all three compounds.

Assignment of Electronic States. For assignment of paramagnetic charge states, the EPR method is most suitable,[10,20] especially when it used in conjunction with calculated spin densities.[21] Both the *g* factor anisotropy as affected by the spin−orbit coupling constant of the heavy metal and the hyperfine coupling, if resolved, can provide information on the distribution of spin between metal and ligand.[10,20−22]

The paramagnetic complex **1** may be tentatively formulated as a ruthenium(III) complex with three monoanionic chelate ligands, two $acac^-$ ligands, and one formazanate. However, both the EPR spectra in fluid and frozen solution (Figure 5, Table 6) and the DFT calculated spin densities (Figure 6, Table 7) indicate a significant contribution (spin density of 0.303) from the formazane ligand at the spin distribution. The isotropic

Table 2. Selected Experimental and DFT Calculated Bond Lengths (Å) for 2^n (Molecule A)

	X-ray	DFT			
bond lengths	$\mathbf{2}^+$	$\mathbf{2}^{2+}$ (S = 1/2)	$\mathbf{2}^+$ (S = 0)	**2** (S = 1/2)	$\mathbf{2}^-$ (S = 1)
Ru1−N2	2.031(5)	2.071	2.084	2.083	2.088
Ru1−N4	2.052(5)	2.062	2.086	2.084	2.088
Ru1−N5	2.112(5)	2.155	2.157	2.143	2.138
Ru1−N6	2.071(5)	2.126	2.112	2.112	2.119
Ru1−N7	2.083(5)	2.127	2.112	2.113	2.119
Ru1−N8	2.096(6)	2.160	2.155	2.142	2.138
N1−N2	1.288(8)	1.285	1.292	1.294	1.296
N3−N4	1.301(7)	1.284	1.292	1.294	1.297
C8−N1	1.365(9)	1.361	1.348	1.348	1.350
C8−N3	1.352(9)	1.365	1.347	1.348	1.350
C9−N4	1.450(8)	1.447	1.440	1.436	1.433
C15−N2	1.488(9)	1.443	1.440	1.436	1.433
C1−C2	1.531(12)	1.502	1.511	1.511	1.512
C2−C3	1.425(13)	1.410	1.401	1.401	1.401
C2−C7	1.338(13)	1.411	1.401	1.401	1.401
C3−C4	1.402(12)	1.383	1.393	1.393	1.393
C4−C5	1.369(11)	1.419	1.405	1.406	1.408
C5−C6	1.411(10)	1.420	1.404	1.406	1.408
C5−C8	1.522(10)	1.457	1.492	1.492	1.489
C6−C7	1.376(11)	1.383	1.393	1.393	1.393

DOI: 10.1021/acs.inorgchem.5b01408
Inorg. Chem. 2015, 54, 8126−8135

Table 3. Selected Experimental and DFT Calculated Bond Lengths (Å) for 3^n

	X-ray	DFT			
bond lengths	3^+	3^{2+} (S = 1/2)	3^+ (S = 0)	**3** (S = 1/2)	3^- (S = 1)
Ru1−N2	2.067(6)	2.080	2.084	2.081	2.089
Ru1−N4	2.081(6)	2.093	2.084	2.081	2.092
Ru1−N5	2.063(4)	2.115	2.101	2.096	2.110
Ru1−N7	2.045(5)	2.161	2.164	2.154	2.172
Ru1−N8	2.050(4)	2.207	2.168	2.159	2.174
Ru1−N9	2.075(4)	2.113	2.100	2.095	2.110
N1−N2	1.243(8)	1.283	1.290	1.292	1.294
N3−N4	1.268(8)	1.282	1.290	1.292	1.294
C8−N1	1.446(8)	1.364	1.346	1.347	1.349
C8−N3	1.398(8)	1.361	1.346	1.347	1.348
C9−N4	1.456(8)	1.438	1.442	1.438	1.435
C15−N2	1.462(9)	1.443	1.442	1.437	1.436
C1−C2	1.531(11)	1.501	1.510	1.511	1.512
C2−C3	1.379(10)	1.412	1.402	1.401	1.401
C2−C7	1.382(10)	1.412	1.401	1.401	1.401
C3−C4	1.389(10)	1.382	1.392	1.393	1.393
C4−C5	1.408(9)	1.420	1.405	1.406	1.407
C5−C6	1.404(9)	1.420	1.404	1.405	1.408
C5−C8	1.474(9)	1.455	1.491	1.492	1.490
C6−C7	1.391(9)	1.382	1.393	1.393	1.393
N6−N7	1.305(6)	1.275	1.280	1.308	1.340
N8−N10	1.291(6)	1.274	1.279	1.309	1.340

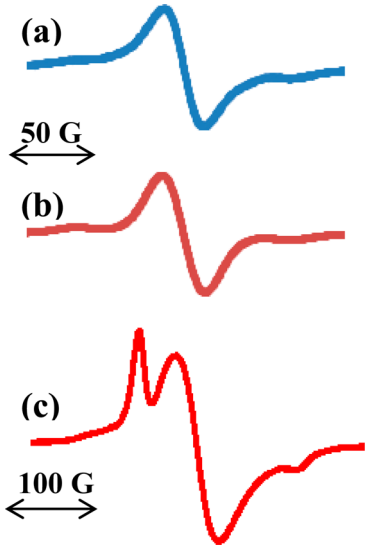

Figure 5. The X-band EPR spectra of **1** at room temperature (a) with simulation (b) and at 100 K (c) in CH_2Cl_2.

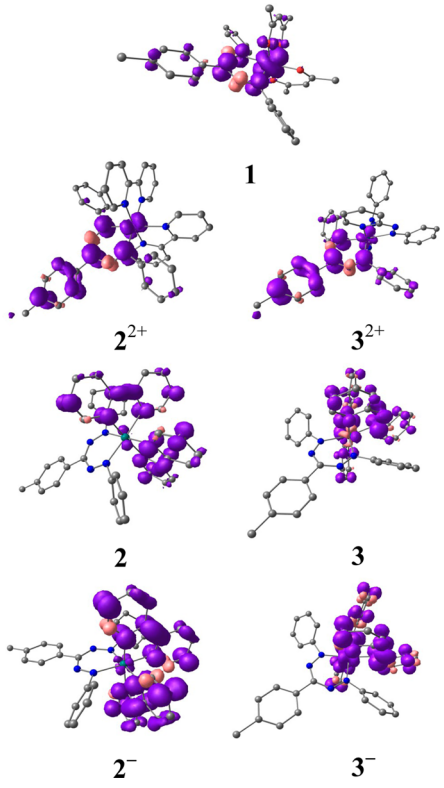

Figure 6. Spin density representations of **1** (S = 1/2), $\mathbf{2}^{2+}$ (S = 1/2), **2** (S = 1/2), $\mathbf{2}^-$ (S = 1), $\mathbf{3}^{2+}$ (S = 1/2), **3** (S = 1/2), and $\mathbf{3}^-$ (S = 1).

^{99,101}Ru hyperfine coupling of about 20 G lies between the values for radical complexes of diamagnetic ruthenium of a few gauss[23] and the approximately 30 G expected for a pure Ru^{III} species.[24] The natural abundancies are 12.7% for ^{99}Ru (I = 5/2) and 17.0% for ^{101}Ru (I = 5/2), and the gyromagnetic ratio is 1.12 in favor of the heavier isotope.[25] The isotropic hyperfine constants a_o are 705.2 and 629.4 G, respectively.[25] The relatively high ^{99,101}Ru hyperfine splitting despite significant spin density on the ligand is a result of the chelate coordination of the metal by two centers (N2, N4) with high spin populations (Figures S6 and S7). Similarly, the g factor anisotropy as measured by g_1-g_3 = 0.13 is situated between that of genuine ruthenium(III) species (>0.5) and the typical values for radical complexes of Ru^{II} (<0.1).[21a] The necessity to describe a $[Ru^n(Q^m)]^k$ charge form with more than one integer oxidation state combination has been pointed out earlier on the basis of experiment[21a] and theory.[21b] Kaupp and Remenyi have thus stated that "The true situation in a given complex may be intermediate between integer oxidation numbers."[21b] Alternatives for oxidation and reduction of **1** (Scheme 1) lead to

DOI: 10.1021/acs.inorgchem.5b01408
Inorg. Chem. 2015, 54, 8126−8135

Table 4. DFT Calculated ((U)B3LYP/6-31G*) Bond Lengths (Å) for L^n

	DFT		
bond lengths	$L^{\bullet}$ (S = 1/2)	L^{-} (S = 0)	$L^{\bullet 2-}$ (S = 1/2)
N1–N2	1.276	1.286	1.341
N3–N4	1.276	1.304	1.341
C8–N1	1.357	1.378	1.359
C8–N3	1.356	1.354	1.353
C9–N4	1.400	1.397	1.363
C15–N2	1.400	1.409	1.356
C1–C2	1.510	1.511	1.512
C2–C3	1.402	1.400	1.405
C2–C7	1.402	1.402	1.403
C3–C4	1.390	1.393	1.392
C4–C5	1.407	1.409	1.414
C5–C6	1.406	1.409	1.413
C5–C8	1.470	1.481	1.489
C6–C7	1.391	1.391	1.393

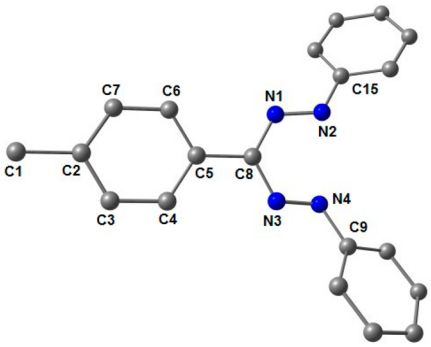

L^n

Scheme 1. Redox Transitions with Assignments of the Most Appropriate Oxidation States

$[Ru^{III}(L^{\bullet})(acac)_2]^+$ / $[Ru^{IV}(L^{-})(acac)_2]^+$		
$-e^- \rightleftharpoons +e^-$		
$[Ru^{III}(L^{-})(acac)_2]$ / $[Ru^{II}(L^{\bullet})(acac)_2]$ / $[Ru^{IV}(L^{\bullet 2-})(acac)_2]$	$[Ru^{III}(L^{-})(bpy)_2]^{2+}$ / $[Ru^{II}(L^{\bullet})(bpy)_2]^{2+}$	$[Ru^{II}(L^{\bullet})(pap)_2]^{2+}$
$-e^- \rightleftharpoons +e^-$	$-e^- \rightleftharpoons +e^-$	$-e^- \rightleftharpoons +e^-$
$[Ru^{II}(L^{-})(acac)_2]^-$ / $[Ru^{III}(L^{\bullet 2-})(acac)_2]^-$	$[Ru^{II}(L^{-})(bpy)_2]^+$	$[Ru^{II}(L^{-})(pap)_2]^+$
	$-e^- \rightleftharpoons +e^-$	$-e^- \rightleftharpoons +e^-$
	$[Ru^{II}(L^{-})(bpy^{\bullet -})(bpy)]$	$[Ru^{II}(L^{-})(pap^{\bullet -})(pap)]$
	$-e^- \rightleftharpoons +e^-$	$-e^- \rightleftharpoons +e^-$
	$[Ru^{II}(L^{-})(bpy^{\bullet -})_2]^-$	$[Ru^{II}(L^{-})(pap^{\bullet -})_2]^-$
$\mathbf{1}^n$	$\mathbf{2}^n$	$\mathbf{3}^n$

EPR silent products and are discussed in the UV–vis–NIR spectroelectrochemistry section.

A similar metal/ligand spin-mixed EPR response with slightly lower g anisotropy and metal hyperfine coupling than for **1** is observed for the in situ electrochemically oxidized complex $\mathbf{2}^{2+}$ (Figure 8, Table 6), although the DFT calculations predict largely ligand-based spin (Figure 6, Table 7). The experiment, however, clearly demonstrates sizable contributions from the

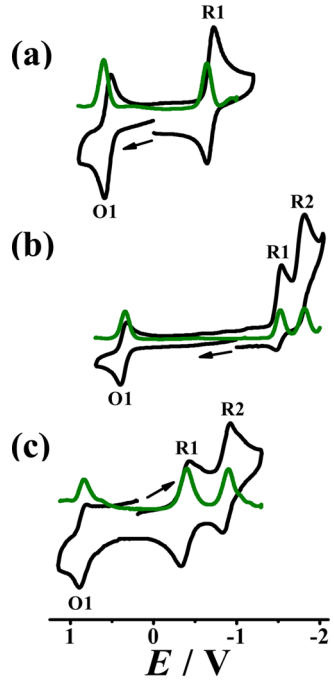

Figure 7. Cyclic (black) and differential pulse (green) voltammograms of (a) **1**, (b) [**2**]ClO_4, and (c) [**3**]ClO_4 in CH_3CN/0.1 M Et_4NClO_4 versus SCE; scan rate 100 mV s^{-1}.

Table 5. Electrochemical Data[a]

	E°_{298}/V (ΔE/mV)[b]			K_c[c]	
compd	Ox	Red1	Red2	K_{c1}[d]	K_{c2}[e]
1	0.55(70)	−0.68(80)		$10^{20.8}$	
[**2**]ClO_4	0.36(70)	−1.51(60)	−1.78(70)	$10^{31.6}$	$10^{4.6}$
[**3**]ClO_4	0.86(70)	−0.38(80)	−0.88(90)	$10^{21.0}$	$10^{8.5}$

[a]From cyclic voltammetry in CH_3CN/0.1 M Et_4NClO_4/GC at 100 mV s^{-1}. [b]Potential in V versus SCE; peak potential differences ΔE/mV (in parentheses). [c]Comproportionation constant from RT ln K_c = $nF(\Delta E)$. [d]K_{c1} between Ox and Red1. [e]K_{c2} between Red1 and Red2.

$Ru^{III}(L^{-})$ combination (Scheme 1). Reduction to neutral **2** produces a hyperfine-split spectrum (Figure S8), which agrees with calculated ligand-based spin (Table 7). Oxidation and reduction of $\mathbf{3}^+$ produce single-line EPR signals (Figures S9,S10) with $g > 2$ for $\mathbf{3}^{2+}$, pointing to $L^{\bullet}$ as a ligand, and with $g < 2$ for **3**, suggesting the reduction of a pap coligand (Figure 6).[26] The Ru^{II}-stabilizing effect of the pap coligands in $\mathbf{3}^n$ leaves only the formazanate available for oxidation to a formazanyl ligand ($L^{-} \rightarrow L^{\bullet}$), demonstrating the two-way noninnocence of L^{-} in either reduction (to $L^{\bullet 2-}$)[6] or oxidation (to $L^{\bullet}$).

According to the DFT calculations, the spin density on the metal is only 10% in $\mathbf{3}^{2+}$ (Table 7). The spin density distribution within the coordinated formazanyl ligand $L^{\bullet}$ in that state is shown in Figure S11, revealing the largest contributions from N2, N4, C8, and the *para*-positioned carbon within the *p*-tolyl ring (each with about 20% spin density). This result suggests a significant role of the aryl substitution in accommodating the spin, stabilizing the oxidized form $L^{\bullet}$, and favoring noninnocence of this frequently used[6,8] formazan ligand.

This is to note that oxidation of free (noncoordinated) formazans has long been known to give (depending on conditions) tetrazolinyl radicals or tetrazolium cations, both of

DOI: 10.1021/acs.inorgchem.5b01408
Inorg. Chem. 2015, 54, 8126–8135

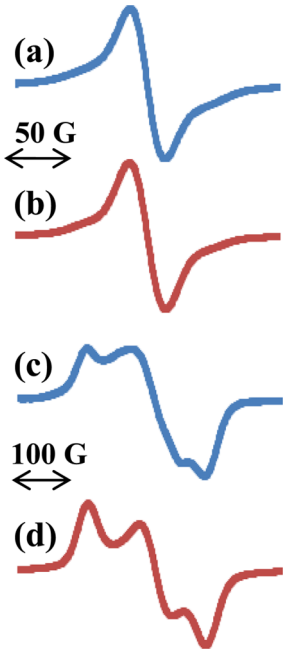

Figure 8. The X-band EPR spectra of electrogenerated 2^{2+} at room temperature (a) with simulation (b) and at 120 K (c) with simulation (d) in CH_2Cl_2/0.1 M $BuNPF_6$.

Table 6. EPR Data[a]

	g_{iso}	g_1	g_2	g_3	g_1-g_3
1	2.022[b]	2.070	2.020	1.94	0.13
$\mathbf{2}^{2+}$	2.021[c]	2.097	2.017	1.96	0.137
2	2.004[d]	[e]	[e]	[e]	[e]
$\mathbf{3}^{2+}$	2.001[e]	2.01	2.002	1.99	0.02
3	1.99[e]	2.00	2.00	1.98	0.02

[a]Measurements in CH_2Cl_2/0.1 M Bu_4NPF_6. g_{iso} values at 293 K, g_1-g_3 determined from frozen solution spectra at 120 K. [b]$a(^{99,101}Ru)$ = 23 G. [c]$a(^{99,101}Ru)$ = 15 G. [d]Hyperfine-split signal, insufficiently resolved. [e]Not resolved.

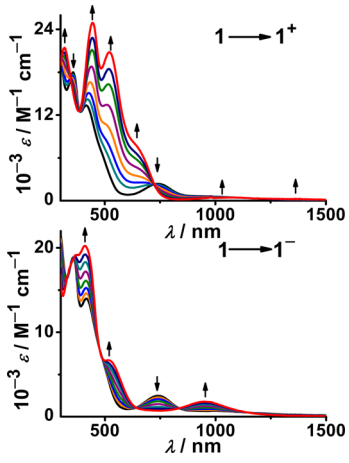

Figure 9. UV−vis−NIR spectroelectrochemistry of $\mathbf{1}^n$ in CH_3CN/0.1 M Bu_4NClO_4.

which result from NN bond formation, which clearly is not possible when formazan is metal-bound.[27] This redox chemistry associated with formazans has long been utilized in cell staining applications.[28]

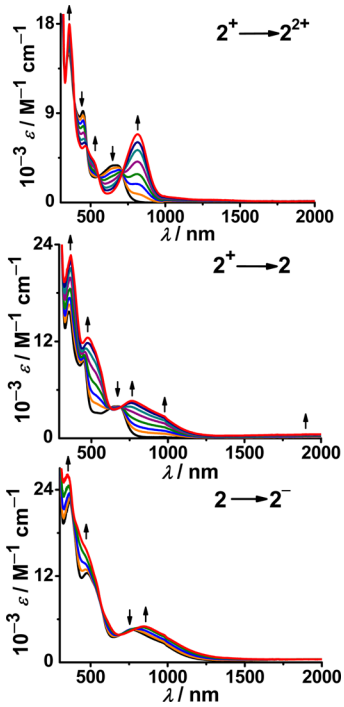

Figure 10. UV−vis−NIR spectroelectrochemistry of $\mathbf{2}^n$ in CH_3CN/0.1 M Bu_4NClO_4.

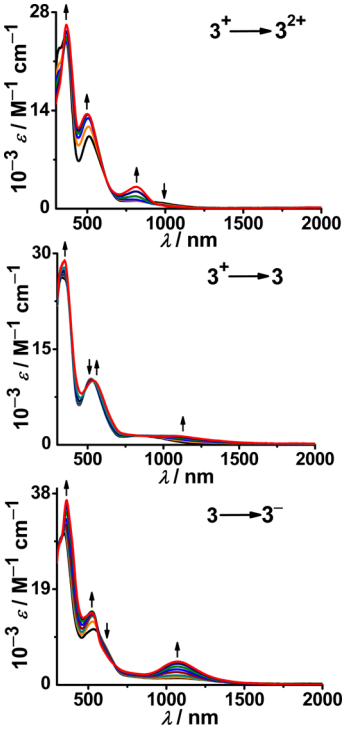

Figure 11. UV−vis−NIR spectroelectrochemistry of $\mathbf{3}^n$ in CH_3CN/0.1 M Bu_4NClO_4.

Those charge states that could not be ascertained through structure determination or EPR spectroscopy can be investigated, as all others, by UV−vis−NIR spectroelectrochemistry in conjunction with TD-DFT calculation results. Figures 9−11 and Tables S8−S10 illustrate good agreement between experimental and calculated data for the major low-energy transitions.

DOI: 10.1021/acs.inorgchem.5b01408
Inorg. Chem. 2015, 54, 8126−8135

Table 7. DFT Calculated (UB3LYP/LanL2DZ/6-31G*) Mulliken Spin Densities

	Ru	L	coligands
1 (S = 1/2)	0.632	0.303	0.065 ($acac^-$)
$\mathbf{2}^{2+}$ (S = 1/2)	0.159	0.847	−0.006 (bpy)
2 (S = 1/2)	0.018	0.007	0.975 (bpy)
$\mathbf{2}^-$ (S = 1)	0.036	0.036	1.928 (bpy)
$\mathbf{3}^{2+}$ (S = 1/2)	0.098	0.901	0.001 (pap)
3 (S = 1/2)	−0.005	−0.017	1.022 (pap)
$\mathbf{3}^-$ (S = 1)	0.147	0.005	1.848 (pap)

On the basis of these results and supported by the earlier discussed EPR information, the major low-energy transitions of the accessible charge states can be identified. The assignments reflect the oxidation state descriptions as listed in Scheme 1. Neutral **1**, for example, formulated as a Ru^{III} species, exhibits an absorption of medium intensity at 740 nm, which is reproduced in agreement with a mainly LMCT (ligand-to-metal charge transfer) transition (with some MLCT admixture). On reduction to $\mathbf{1}^-$ the MLCT (metal-to-ligand charge transfer) character dominates, confirming the ruthenium(II) assignment. A more mixed situation prevails for $\mathbf{1}^+$ with correspondingly complex transition assignments (Figure 9, Table S8).

The system $\mathbf{2}^n$ is characterized by MLCT/LLCT (ligand-to-ligand charge transfer) bands for the monocation, with π^*(bpy) as target MO (Figure 10, Table S9). On oxidation to $\mathbf{2}^{2+}$, a relatively intense HOMO → LUMO absorption band emerges at 815 nm with intraligand (IL) characteristics. Reduction, on the other hand, reveals several ligand-to-ligand transitions, in addition to the well-known IL band of bpy radical anion in the near-infrared.[29] The second reduction shows a relatively small change, confirming the reduction of the second 2,2′-bipyridine ligand.

The series $\mathbf{3}^n$ (Figure 11, Table S10) displays a behavior similar to that of $\mathbf{2}^n$, regarding the NIR absorption after oxidation. Mixed transitions involving mainly both types of noninnocent ligands are responsible for the near IR absorption of the neutral and monoanionic forms of $\mathbf{3}^n$. From these data and the underlying frontier MO identification, one can confirm the structurally and EPR spectroscopically derived oxidation state assignments and add the missing information in Scheme 1. According to this, the reduction of **1** occurs mostly on the metal, yielding a $Ru^{II}(L^-)$ species (Scheme 1). Oxidation of **1** proceeds on L^- as well as on the metal (SOMO of **1**, 65% L, 25% Ru; and LUMO of $\mathbf{1}^+$, 51% L, 37% Ru) to produce the spin-paired complex containing $Ru^{III}(L^\bullet)$ (antiferromagnetically coupled) and closed shell $Ru^{IV}(L^-)$ contributions, in agreement with the stability of $[Ru^{IV}(acac)_2]^{2+}$[30] ($E(S = 1) - E(S = 0)$ = 2200 cm^{-1} for $\mathbf{1}^+$, Table S22). Further, the calculated identical energy of broken symmetry singlet and closed shell singlet of $\mathbf{1}^+$ signifies the appreciable contribution of $Ru^{IV}L^-$.

In the series of $\mathbf{2}^n$ and $\mathbf{3}^n$, the oxidation of the isolated cations yields either a metal ($\mathbf{2}^{2+}$) or a formazanate-centered process ($\mathbf{3}^{2+}$), reflecting the particular stabilization of ruthenium(II) by strongly π-accepting pap. In both cases, the reduction to the neutral form occurs at the reducible neutral coligands (bpy or pap) and not at the anionic formazanate, in contrast to zinc(II) complexes $[Zn(L)_2]^n$.[6]

CONCLUSION

We have shown that formazanate ligands can not only be reduced beyond the conventional monoanionic state[6] but can also undergo oxidation to the neutral formazanyl form within metal complexes (Scheme 2), evident from the conversion of $[Ru^{II}(L^-)(pap)_2]^+$ to $[Ru^{II}(L^\bullet)(pap)_2]^{2+}$ instead of $[Ru^{III}(L^-)(pap)_2]^{2+}$.

Scheme 2. Formazanate Ligand Redox System

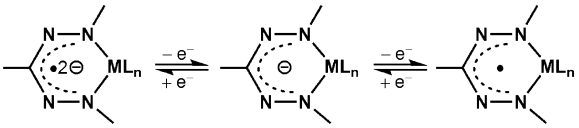

They are thus truly noninnocently behaving ligands in more than one way ("bidirectional"),[17b] complementing the still small number of redox-active ligands able to act within six-membered chelate ring situations.[16−18] These include β-diketonates with anellated aromatic rings as in 9-oxidophenalenone[17] or β-diketiminates.[16] The related verdazyl radical ligands[4] were also shown to exhibit noninnocent behavior of six-memebered ring chelates. Future studies of combinations between formazanates and metals other than zinc[6] or ruthenium will have to illustrate as to which situations favor oxidation or reduction of these coordinated redox-active ligands.

EXPERIMENTAL SECTION

Materials. The precursor complexes *cis*-$Ru(acac)_2(CH_3CN)_2$,[31] *cis*-$Ru(bpy)_2Cl_2$,[32] *ctc*-$Ru(pap)_2Cl_2$,[33] and the ligand 1,5-diphenyl-3-*p*-tolylformazan[8c] (HL) were prepared according to the literature procedures. Other chemicals and solvents were of reagent grade and used as received. For spectroscopic and electrochemical studies, HPLC grade solvents were used.

Physical Measurements. The electrical conductivity of solutions was checked using an autoranging conductivity meter (Toshcon Industries, India). The EPR measurements were made in a two-electrode capillary tube[34] with an X-band (9.5 GHz) Bruker system ESP300 spectrometer. Cyclic voltammetric and differential pulse voltammetric measurements of the complexes were done using a PAR model 273A electrochemistry system. Glassy carbon working, platinum wire auxiliary electrode, and saturated calomel reference electrode (SCE) were used in a standard three-electrode configuration with tetraethylammonium perchlorate (TEAP) as the supporting electrolyte (substrate concentration ≈ 10^{-3} M; standard scan rate 100 mV s^{-1}). (***Caution!*** *Perchlorate salts are explosive and should be handled with care.*) UV−vis−NIR spectroelectrochemical studies were performed in CH_3CN/0.1 M Bu_4NPF_6 at 298 K using an optically transparent thin-layer electrode (OTTLE) cell[35] mounted in the sample compartment of a J&M TIDAS spectrophotometer. All spectroelectrochemical experiments were carried out under a dinitrogen atmosphere. ^1H NMR spectra were recorded on a Bruker Avance III 400 MHz spectrometer. The elemental analyses were recorded on a PerkinElmer 240C elemental analyzer. Electrospray mass spectral measurements were done on a Micromass Q-ToF mass spectrometer.

Preparation of Complexes. *Synthesis of [Ru(L⁻)(acac)₂] (1).* The precursor *cis*-$Ru(acac)_2(CH_3CN)_2$ (100 mg, 0.26 mmol) and the ligand HL (82 mg, 0.26 mmol) were dissolved in 50 mL of C_2H_5OH, upon which NEt_3 (0.045 mL, 0.27 mmol) was added to the solution, followed by refluxing for 8 h under aerobic reaction condition. The solvent was removed and the product was purified using a silica gel column, and the yellowish-brown complex **1** was eluted by a 2:1 CH_2Cl_2:hexane mixture. The solvent was removed to yield pure **1**. Yield, 116 mg (72%). MS (ESI+, CH_3CN): m/z $\{\mathbf{1}\}^+$ calcd, 612.67; found, 613.04. ^1H NMR (400 MHz) in $CDCl_3$ [δ/ppm (J/Hz)]: 8.43 (d, 8, 1H), 8.35 (d, 8, 1H), 8.12 (d, 8, 2H), 7.73 (m, 1H), 7.44 (m, 6H), 7.16 (d, 8, 3H), 2.44 (s, 1H), 2.42 (s, 3H), 2.39 (s, 1H), 2.37 (s, 3H), 2.18 (s, 3H), 2.11 (s, 3H), 1.96 (s, 3H). ^{13}C NMR (400 MHz) in $CDCl_3$ [δ/ppm]: 129.55, 129.30, 128.85, 128.65, 126.60, 125.50, 124.11, 56.20, 32.00, 31.90, 22.65, 21.50, 14.10, −9.80. Anal. Calcd for

DOI: 10.1021/acs.inorgchem.5b01408
Inorg. Chem. 2015, 54, 8126−8135

$C_{30}H_{31}N_4O_4Ru$: C, 58.81; H, 5.10; N, 9.14. Found: C, 58.88; H, 5.23; N, 8.97. Molar conductivity (CH_3CN): Λ_M = 5 Ω^{-1} cm^2 M^{-1}.

*Synthesis of [Ru(L$^-$)(bpy)$_2$]ClO$_4$ ([**2**]ClO$_4$).* The starting complexes *cis*-Ru(bpy)$_2$Cl$_2$ (100 mg, 0.21 mmol) and AgClO$_4$ (87.07 mg, 0.42 mmol) were taken in EtOH and refluxed for 2 h. The precipitated AgCl was filtered off through a sintered Gooch crucible. The filtrate was then treated with HL (66 mg, 0.21 mmol) and NEt$_3$ (0.035 mL, 0.21 mmol). The mixture was refluxed for 10 h under dinitrogen atmosphere. The solvent was removed, and the residue was moistened with a few drops of CH_3CN followed by the addition of a saturated aqueous solution of NaClO$_4$. After being stored at 273 K overnight, the precipitate was filtered and washed with chilled water to remove excess NaClO$_4$ and dried in vacuo over P_4O_{10}. The product was purified using a silica gel column, and the green complex [**2**]ClO$_4$ was eluted by 4:1 CH_2Cl_2:CH_3CN mixture. The solvent was removed to yield pure [**2**]ClO$_4$. Yield, 109 mg (64%). MS (ESI+, CH_3CN): *m*/*z* {**2**}$^+$ calcd, 726.83; found, 727.01. ^{1}H NMR (400 MHz) in $CDCl_3$ [δ/ppm (*J*/Hz)]: 8.95 (d, 8, 2H), 8.2 (d, 8, 2H), 8.09 (m, 2H), 7.86 (d, 8, 2H), 7.74 (d, 8, 2H), 7.55 (m, 6H), 7.08 (d, 8, 2H), 7.03 (t, 8, 2H), 6.75 (m, 6H), 6.28 (d, 8, 4H), 2.32 (s, 3H). ^{13}C NMR (400 MHz) in $CDCl_3$ [δ/ppm]: 157.16, 155.68, 151.19, 143.74, 137.94, 136.98, 133.82, 133.61, 130.36, 130.16, 129.16, 128.40, 127.55, 126.75, 126.55, 126.23, 123.90, 122.96, 29.58, 22.81. Anal. Calcd for $C_{40}H_{33}N_8O_4ClRu$: C, 58.10; H, 4.03; N, 13.56. Found: C, 57.91; H, 4.11; N, 13.77. Molar conductivity (CH_3CN): Λ_M = 87 Ω^{-1} cm^2 M^{-1}.

*Synthesis of [Ru(L$^-$)(pap)$_2$]ClO$_4$ ([**3**]ClO$_4$).* The starting complex *cis*−*trans*−*cis*-Ru(pap)$_2$Cl$_2$ (100 mg, 0.19 mmol) and AgClO$_4$ (79.04 mg, 0.38 mmol) were taken in EtOH and refluxed for 2 h. The precipitated AgCl was filtered off through a sintered Gooch crucible. The filtrate was treated with HL (60 mg, 0.19 mmol) and NEt$_3$ (0.035 mL, 0.21 mmol). The mixture was refluxed for 8 h, and then the solvent was removed. The residue was moistened with a few drops of CH_3CN followed by the addition of saturated aqueous solution of NaClO$_4$. After being stored at 273 K overnight, the precipitate was filtered, washed with chilled water to remove excess NaClO$_4$, and dried in vacuo over P_4O_{10}. The product was purified using a silica gel column, and the dark violet complex [**3**]ClO$_4$ was eluted by a 5:1 CH_2Cl_2:CH_3CN mixture. Yield, 111 mg (68%). MS (ESI+, CH_3CN): *m*/*z* {**3**}$^+$ calcd, 780.88; found, 781.23. ^{1}H NMR (400 MHz) in $(CD_3)_2SO$ [δ/ppm (*J*/Hz)]: 8.88 (d, 6, 2H), 8.57 (d, 6, 2H), 8.40 (t, 7.5, 2H), 7.88 (m, 2H), 7.63 (d, 10, 2H), 7.43 (m, 2H), 7.20 (d, 6, 2H), 7.15 (t, 10, 4H), 7.1 (t, 7.5, 3H), 7.00 (t, 7.5, 4H), 6.67 (m, 7H), 2.32 (s, 3H). ^{13}C NMR (400 MHz) in $(CD_3)_2SO$ [δ/ppm]: 164.40, 155.16,152.27, 150.31, 144.94, 140.71, 135.32, 133.08, 129.04, 128.71, 128.14, 127.76, 127.35, 124.66, 123.79, 123.28, 123.18, 54.87, 20.75. Anal. Calcd for $C_{42}H_{35}N_{10}O_4ClRu$: C, 57.26; H, 4.01; N, 15.91. Found: C, 57.53; H, 4.06; N, 15.58. Molar conductivity (CH_3CN): Λ_M = 92 Ω^{-1} cm^2 M^{-1}.

(***Caution!*** *Perchlorate salts are explosive and should be handled with care.*)

Crystal Structure Determination. Single crystals of **1**, [**2**]ClO$_4$, and [**3**]ClO$_4$ were grown by slow evaporation of 1:1 CH_2Cl_2−hexane, CH_2Cl_2−toluene, and $CHCl_3$−CH_3OH solutions, respectively. X-ray diffraction data were collected using a Rigaku Saturn-724+ CCD single-crystal diffractometer using Mo Kα radiation. The data collection was evaluated by using the CrystalClear-SM Expert software. The data were collected by the standard ω-scan technique. The structure was solved by direct method using SHELXS-97 and refined by full matrix least-squares with SHELXL-97, refining on F^2.[36] All data were corrected for Lorentz and polarization effects, and all non-hydrogen atoms were refined anisotropically. The remaining hydrogen atoms were placed in geometrically constrained positions and refined with isotropic temperature factors, generally 1.2U_{eq} of their parent atoms. Hydrogen atoms were included in the refinement process as per the riding model. SQUEEZE was applied for the disordered unidentified solvent molecule in the crystal of [**2**]ClO$_4$.

Computational Details. Full geometry optimizations were carried out using the density functional theory method at the (U)B3LYP level for **1**^{n} (*n* = 0), **2**^{n} (*n* = 2+, 0, −), and **3**^{n} (*n* = 2+, 0, −) and (R)B3LYP for **1**^{n} (*n* = +, −), **2**^{n} (*n* = +), and **3**^{n} (*n* = +).[37] All elements except ruthenium were assigned the 6-31G(d) basis set. The LanL2DZ basis set with effective core potential was employed for the ruthenium atom.[38] All calculations were performed with the Gaussian 09 program package.[39] Vertical electronic excitations based on (U)B3LYP optimized geometries were computed using the time-dependent density functional theory (TD-DFT) formalism[40] in acetonitrile using the conductor-like polarizable continuum model (CPCM).[41] Chemissian 1.7[42] was used to calculate the fractional contributions of various groups to each molecular orbital. All calculated structures were visualized with ChemCraft.[43]

■ ASSOCIATED CONTENT

Supporting Information

The Supporting Information is available free of charge on the ACS Publications website at DOI: 10.1021/acs.inorgchem.5b01408. CCDC-1406591 (**1**), CCDC-1406592 ([**2**]ClO$_4$), and CCDC-1406593 ([**3**]ClO$_4$) contain the supplementary crystallographic data for this Article. These data can be obtained free of charge from The Cambridge Crystallographic Data Centre via www.ccdc.cam.ac.uk/data_request/cif.

X-ray data for compound **1** (CIF)
X-ray data for compound [**2**]ClO$_4$ (CIF)
X-ray data for compound [**3**]ClO$_4$ (CIF)
Mass spectra (Figure S1), crystal (Figure S2), ^{1}H NMR (Figure S3), ^{13}C NMR (Figure S4), DFT optimized structures (Figure S5), spin density on specific atoms (Figures S6, S7, and S11), EPR (Figures S8−S10), crystal data and DFT (Tables S1−S7), TD-DFT (Tables S8−S10), and MO compositions and energies (Tables S11−S24) (PDF)

■ AUTHOR INFORMATION

Corresponding Authors

*E-mail: kaim@iac.uni-stuttgart.de.
*E-mail: lahiri@chem.iitb.ac.in.

Notes

The authors declare no competing financial interest.

■ ACKNOWLEDGMENTS

Financial support received from the Department of Science and Technology, Council of Scientific and Industrial Research (fellowship to A.M.), New Delhi (India), the Land Baden-Württemberg (Germany), and the Czech Republic (grant 14-05180S) is gratefully acknowledged.

■ REFERENCES

(1) Kaim, W. *Inorg. Chem.* **2011**, *50*, 9752−9765.
(2) Kaim, W. *Coord. Chem. Rev.* **2002**, *230*, 127−139.
(3) (a) Kaim, W. *Coord. Chem. Rev.* **2001**, *219*−*221*, 463−488. (b) Das, A.; Scherer, T. M.; Mobin, S. M.; Kaim, W.; Lahiri, G. K. *Chem. - Eur. J.* **2012**, *18*, 11007−11018. (c) Sarkar, B.; Patra, S.; Fiedler, J.; Sunoj, R. B.; Janardanan, D.; Lahiri, G. K.; Kaim, W. *J. Am. Chem. Soc.* **2008**, *130*, 3532−3542. (d) Ehret, F.; Bubrin, M.; Hübner, R.; Schweinfurth, D.; Hartenbach, I.; Záliš, S.; Kaim, W. *Inorg. Chem.* **2012**, *51*, 6237−6244.
(4) Gilroy, J. B.; McKinnon, S. D. J.; Koivisto, B. D.; Hicks, R. G. *Org. Lett.* **2007**, *9*, 4837−4840.
(5) Ehret, F.; Bubrin, M.; Záliš, S.; Kaim, W. *Angew. Chem.* **2013**, *125*, 4771−4773; *Angew. Chem., Int. Ed.* **2013**, *52*, 4673−4675.
(6) (a) Chang, M.-C.; Dann, T.; Day, D. P.; Lutz, M.; Wildgoose, G. G.; Otten, E. *Angew. Chem.* **2014**, *126*, 4202−4206; *Angew. Chem., Int. Ed.* **2014**, *53*, 4118−4122. (b) Chang, M.-C.; Roewen, P.; Travieso-Puente, R.; Lutz, M.; Otten, E. *Inorg. Chem.* **2015**, *54*, 379−388.

DOI: 10.1021/acs.inorgchem.5b01408
Inorg. Chem. 2015, 54, 8126−8135

(7) (a) Grychtol, K.; Mennicke, W. *Ullmann's Encyclopedia of Industrial Chemistry*; Wiley: New York, 2012; pp 595−633. (b) Zollinger, H. *Color Chemistry*, 3rd ed.; Wiley-VCH: Weinheim (Germany), 2003. (c) Ried, W. *Angew. Chem.* **1952**, *64*, 391−396.
(8) (a) Chang, M.-C.; Otten, E. *Chem. Commun.* **2014**, *50*, 7431−7433. (b) Barbon, S. M.; Price, J. T.; Reinkeluers, P. A.; Gilroy, J. B. *Inorg. Chem.* **2014**, *53*, 10585−10593. (c) Gilroy, J. B.; Ferguson, M. J.; McDonald, R.; Patrick, B. O.; Hicks, R. G. *Chem. Commun.* **2007**, 126−128. (d) Kawamura, Y.; Yamauchi, J.; Azuma, N. *Acta Crystallogr., Sect. B: Struct. Sci.* **1997**, *B53*, 451−456. (e) Siedle, A. R.; Pignolet, L. H. *Inorg. Chem.* **1980**, *19*, 2052−2056. (f) Dale, D. *J. Chem. Soc. A* **1967**, 278−287. (g) Irving, H.; Gill, J. B.; Cross, W. R. *J. Chem. Soc.* **1960**, 2087−2095.
(9) For a related ruthenium compound, see: Jameson, G. B.; Muster, A.; Robinson, S. D.; Wingfield, J. M.; Ibers, J. A. *Inorg. Chem.* **1981**, *20*, 2448−2456.
(10) Kaim, W.; Lahiri, G. K. *Angew. Chem.* **2007**, *119*, 1808−1828; *Angew. Chem., Int. Ed.* **2007**, *46*, 1778−1796.
(11) (a) Lahiri, G. K.; Kaim, W. *Dalton Trans.* **2010**, *39*, 4471−4478. (b) Kaim, W. In *NO_x Related Chemistry*; van Eldik, R., Olabe, J., Eds.; ADIOCH, Academic Press: UK, 2015; Vol. *67*, p S.295.
(12) Grupp, A.; Bubrin, M.; Ehret, F.; Zeng, Q.; Hartl, F.; Kvapilová, H.; S. Záliš, S.; Kaim, W. *Eur. J. Inorg. Chem.* **2014**, *2014*, 110−119.
(13) (a) Das, A.; Ghosh, P.; Plebst, S.; Schwederski, B.; Mobin, S. M.; Kaim, W.; Lahiri, G. K. *Inorg. Chem.* **2015**, *54*, 3376−3386. (b) Das, D.; Scherer, T. M.; Das, A.; Mondal, T. K.; Mobin, S. M.; Fiedler, J.; Priego, J. L.; J.-Aparicio, R.; Kaim, W.; Lahiri, G. K. *Dalton Trans.* **2012**, *41*, 11675−11683. (c) Das, D.; Sarkar, B.; Kumbhakar, D.; Mondal, T. K.; Mobin, S. M.; Fiedler, J.; Urbanos, F. A.; J.-Aparicio, R.; Kaim, W.; Lahiri, G. K. *Chem. - Eur. J.* **2011**, *17*, 11030−11040. (d) Das, D.; Mondal, T. K.; Chowdhury, A. D.; Weisser, F.; Schweinfurth, D.; Sarkar, B.; Mobin, S. M.; Urbanos, F. A.; J.-Aparicio, R.; Kaim, W.; Lahiri, G. K. *Dalton Trans.* **2011**, *40*, 8377−8390. (e) Das, D.; Sarkar, B.; Mondal, T. K.; Mobin, S. M.; Fiedler, J.; Kaim, W.; Lahiri, G. K. *Inorg. Chem.* **2011**, *50*, 7090−7098. (f) Das, D.; Das, A. K.; Sarkar, B.; Mondal, T. K.; Mobin, S. M.; Fiedler, J.; Záliš, S.; Urbanos, F. A.; J.-Aparicio, R.; Kaim, W.; Lahiri, G. K. *Inorg. Chem.* **2009**, *48*, 11853−11864. (g) Das, D.; Mondal, T. K.; Mobin, S. M.; Lahiri, G. K. *Inorg. Chem.* **2009**, *48*, 9800−9810.
(14) Kaim, W.; Fiedler, J. *Chem. Soc. Rev.* **2009**, *38*, 3373−3382.
(15) (a) Praneeth, V. K. K.; Ringenberg, M. R.; Ward, T. R. *Angew. Chem.* **2012**, *124*, 10374−10380; *Angew. Chem., Int. Ed.* **2012**, *51*, 10228−10234. (b) Luca, O. R.; Crabtree, R. H. *Chem. Soc. Rev.* **2013**, *42*, 1440−1459. (c) Dzik, W. I.; de Bruin, B. *Organometallic Chemistry* **2011**, *37*, 46−78. (d) Lyaskovskyy, V.; de Bruin, B. *ACS Catal.* **2012**, *2*, 270−279.
(16) Khusniyarov, M. M.; Bill, E.; Weyhermüller, T.; Bothe, E.; Wieghardt, K. *Angew. Chem.* **2011**, *123*, 1690−1693; *Angew. Chem., Int. Ed.* **2011**, *50*, 1652−1655.
(17) (a) Das, A.; Scherer, T. M.; Mobin, S. M.; Kaim, W.; Lahiri, G. K. *Inorg. Chem.* **2012**, *51*, 4390−4397. (b) Agarwala, H.; Scherer, T. M.; Mobin, S. M.; Kaim, W.; Lahiri, G. K. *Dalton Trans.* **2014**, *43*, 3939−3948.
(18) (a) Ehret, F.; Bubrin, M.; Záliš, S.; Kaim, W. *Z. Anorg. Allg. Chem.* **2014**, *640*, 2781−2787. (b) Ehret, F.; Bubrin, M.; Záliš, S.; Kaim, W. *Chem.—Eur. J.*, in print.
(19) (a) Mandal, A.; Agarwala, H.; Ray, R.; Plebst, S.; Mobin, S. M.; Priego, J. L.; Jiménez-Aparicio, R.; Kaim, W.; Lahiri, G. K. *Inorg. Chem.* **2014**, *53*, 6082−6093. (b) Mandal, A.; Kundu, T.; Ehret, F.; Bubrin, M.; Mobin, S. M.; Kaim, W.; Lahiri, G. K. *Dalton Trans.* **2014**, *43*, 2473−2487. (c) Mondal, P.; Plebst, S.; Ray, R.; Mobin, S. M.; Kaim, W.; Lahiri, G. K. *Inorg. Chem.* **2014**, *53*, 9348−9356. (d) Ghosh, P.; Mondal, P.; Ray, R.; Das, A.; Bag, S.; Mobin, S. M.; Lahiri, G. K. *Inorg. Chem.* **2014**, *53*, 6094−6106.
(20) Ernst, S.; Hänel, P.; Jordanov, J.; Kaim, W.; Kasack, V.; Roth, E. *J. Am. Chem. Soc.* **1989**, *111*, 1733−1738.
(21) (a) Patra, S.; Sarkar, B.; Mobin, S. M.; Kaim, W.; Lahiri, G. K. *Inorg. Chem.* **2003**, *42*, 6469−6473. (b) Remenyi, C.; Kaupp, M. *J. Am. Chem. Soc.* **2005**, *127*, 11399−11413.
(22) Kaim, W. *Coord. Chem. Rev.* **1987**, *76*, 187−235.
(23) (a) Waldhör, E.; Schwederski, B.; Kaim, W. *J. Chem. Soc., Perkin Trans. 2* **1993**, 2109−2111. (b) Kaim, W.; Schwederski, B. In *Magnetic Properties of Free Radicals*; Fischer, H., Ed.; Landolt-Börnstein II/26a, 2006; p 1.
(24) (a) DeSimone, R. E. *J. Am. Chem. Soc.* **1973**, *95*, 6238−6244. (b) Daul, C.; Goursot, A. *Inorg. Chem.* **1985**, *24*, 3554−3558. (c) Rong, C. C.; So, H.; Pope, M. T. *Eur. J. Inorg. Chem.* **2009**, *2009*, 5211−5214.
(25) Weil, J. A.; Bolton, J. R. *Electron Paramagnetic Resonance*, 2nd ed.; Wiley: Hoboken, 2007.
(26) Das, D.; Agarwala, H.; Chowdhury, A. D.; Patra, T.; Mobin, S. M.; Sarkar, B.; Kaim, W.; Lahiri, G. K. *Chem. - Eur. J.* **2013**, *19*, 7384−7394.
(27) (a) Neugebauer, F. A. *Angew. Chem., Int. Ed. Engl.* **1969**, *8*, 520. (b) Umemoto, K. *Bull. Chem. Soc. Jpn.* **1985**, *58*, 2051−2055. (c) González, M. C.; Román, E. S. *J. Phys. Chem.* **1989**, *93*, 3536−3540. (d) Kovacs, A.; Wojnarovits, L.; Baranyai, M.; Moussa, A.; Othman, I.; McLaughlin, W. L. *Radiat. Phys. Chem.* **1999**, *55*, 795−798. (e) Sadeghi, A.; Chaychian, M.; Al-Sheikhly, M.; McLaughlin, W. L. *Radiat. Phys. Chem.* **2002**, *64*, 13−18.
(28) (a) Mosmann, T. *J. Immunol. Methods* **1983**, *65*, 55−63. (b) Denizot, F.; Lang, R. *J. Immunol. Methods* **1986**, *89*, 271−277. (c) Scudiero, D. A.; Shoemaker, R. H.; Paull, K. D.; Monks, A.; Tierney, S.; Nofziger, T. H.; Currens, M. J.; Seniff, D.; Boyd, M. R. *Cancer Res.* **1988**, *48*, 4827−4833. (d) Boulos, L.; Prévost, M.; Barbeau, B.; Coallier, J.; Desjardins, R. *J. Microbiol. Methods* **1999**, *37*, 77−86. (e) Frank, J. A.; Miller, B. R.; Arbab, A. S.; Zywicke, H. A.; Jordan, E. K.; Lewis, B. K.; Bryant, L. H., Jr.; Bulte, J. W. M. *Radiology* **2003**, *228*, 480−487.
(29) (a) Braterman, P. S.; Song, J.-I.; Wimmer, F. M.; Wimmer, S.; Kaim, W.; Klein, A.; Peacock, R. D. *Inorg. Chem.* **1992**, *31*, 5084−5088. (b) Kaim, W.; Reinhardt, R.; Sieger, M. *Inorg. Chem.* **1994**, *33*, 4453−4459.
(30) (a) Agarwala, H.; Scherer, T.; Maji, S.; Mondal, T. K.; Mobin, S. M.; Fiedler, J.; Urbanos, F. A.; Jiménez-Aparicio, R.; Kaim, W.; Lahiri, G. K. *Chem. - Eur. J.* **2012**, *18*, 5667−5675. (b) Kar, S.; Sarkar, B.; Ghumaan, S.; Roy, D.; Urbanos, F. A.; Fiedler, J.; Sunoj, R. B.; J.-Aparicio, R.; Kaim, W.; Lahiri, G. K. *Inorg. Chem.* **2005**, *44*, 8715−8722.
(31) Kobayashi, T.; Nishina, Y.; Shimizu, K. G.; Satô, G. P. *Chem. Lett.* **1988**, 1137−1140.
(32) Sullivan, B. P.; Salmon, D. J.; Meyer, T. J. *Inorg. Chem.* **1978**, *17*, 3334−3341.
(33) Goswami, S.; Chakravarty, A. R.; Chakravorty, A. *Inorg. Chem.* **1983**, *22*, 602−609.
(34) Kaim, W.; Ernst, S.; Kasack, V. *J. Am. Chem. Soc.* **1990**, *112*, 173−178.
(35) Krejcik, M.; Danek, M.; Hartl, F. *J. Electroanal. Chem. Interfacial Electrochem.* **1991**, *317*, 179−187.
(36) (a) Sheldrick, G. M. *Acta Crystallogr., Sect. A* **2008**, *A64*, 112−122. (b) *Program for Crystal Structure Solution and Refinement*; University of Göttingen: Göttingen, Germany, 1997.
(37) Lee, C.; Yang, W.; Parr, R. G. *Phys. Rev. B: Condens. Matter Mater. Phys.* **1988**, *37*, 785−789.
(38) (a) Andrae, D.; Haeussermann, U.; Dolg, M.; Stoll, H.; Preuss, H. *Theor. Chim. Acta* **1990**, *77*, 123−141. (b) Fuentealba, P.; Preuss, H.; Stoll, H.; Szentpaly, L. V. *Chem. Phys. Lett.* **1982**, *89*, 418−422.
(39) Frisch, M. J.; Trucks, G. W.; Schlegel, H. B.; Scuseria, G. E.; Robb, M. A.; Cheeseman, J. R.; Scalmani, G.; Barone, V.; Mennucci, B.; Petersson, G. A.; Nakatsuji, H.; Caricato, M.; Li, X.; Hratchian, H. P.; Izmaylov, A. F.; Bloino, J.; Zheng, G.; Sonnenberg, J. L.; Hada, M.; Ehara, M.; Toyota, K.; Fukuda, R.; Hasegawa, J.; Ishida, M.; Nakajima, T.; Honda, Y.; Kitao, O.; Nakai, H.; Vreven, T.; Montgomery, J. A., Jr.; Peralta, J. E.; Ogliaro, F.; Bearpark, M.; Heyd, J. J.; Brothers, E.; Kudin, K. N.; Staroverov, V. N.; Kobayashi, R.; Normand, J.; Raghavachari, K.; Rendell, A.; Burant, J. C.; Iyengar, S. S.; Tomasi, J.; Cossi, M.; Rega, N.; Millam, J. M.; Klene, M.; Knox, J. E.; Cross, J. B.; Bakken, V.; Adamo, C.; Jaramillo, J.; Gomperts, R.; Stratmann, R. E.; Yazyev, O.;

DOI: 10.1021/acs.inorgchem.5b01408
Inorg. Chem. 2015, 54, 8126−8135

Austin, A. J.; Cammi, R.; Pomelli, C.; Ochterski, J. W.; Martin, R. L.; Morokuma, K.; Zakrzewski, V. G.; Voth, G. A.; Salvador, P.; Dannenberg, J. J.; Dapprich, S.; Daniels, A. D.; Farkas, O.; Foresman, J. B.; Ortiz, J. V.; Cioslowski, J.; Fox, D. J. *Gaussian 09* (revision A.02); Gaussian, Inc.: Wallingford, CT, 2009.
(40) (a) Bauernschmitt, R.; Ahlrichs, R. *Chem. Phys. Lett.* **1996**, *256*, 454−464. (b) Stratmann, R. E.; Scuseria, G. E.; Frisch, M. J. *J. Chem. Phys.* **1998**, *109*, 8218−8225. (c) Casida, M. E.; Jamorski, C.; Casida, K. C.; Salahub, D. R. *J. Chem. Phys.* **1998**, *108*, 4439−4450.
(41) (a) Barone, V.; Cossi, M. *J. Phys. Chem. A* **1998**, *102*, 1995−2001. (b) Cossi, M.; Barone, V. *J. Chem. Phys.* **2001**, *115*, 4708−4718. (c) Cossi, M.; Rega, N.; Scalmani, G.; Barone, V. *J. Comput. Chem.* **2003**, *24*, 669−681.
(42) Leonid, S. *Chemissian 1.7*; 2005−2010. Available at http://www.chemissian.com.
(43) Zhurko, D. A.; Zhurko, G. A. *ChemCraft 1.5*; Plimus: San Diego, CA. Available at http://www.chemcraftprog.com.

DOI: 10.1021/acs.inorgchem.5b01408
Inorg. Chem. 2015, 54, 8126−8135